Acta Biochim Biophys Sin 2022, 54(7): 917–930
https://doi.org/10.3724/abbs.2022080
Advance Access Publication Date: 18 July 2022
Original Article

Original Article

Involvement of PGC7 and UHRF1 in the regulation of DNA methylation of the IG-DMR in the imprinted *Dlk1-Dio3* locus

Mengying Yu[1,2,3,†], Yingxiang Liu[1,2,†], Zhuo Han[1,2,†], Wei Du[1,2], Bingxue Chen[1,2], Lei Zhang[1,2], Hongni Xue[1,2], Zihan Zhang[1,2], and Zekun Guo[1,2,*]

[1]College of Veterinary Medicine, Northwest A&F University, Yangling 712100, China, [2]Key Laboratory of Animal Biotechnology, Ministry of Agriculture, Northwest A&F University, Yangling 712100, China, and [3]Xi'an Center for Disease Control and Prevention, Xi'an 710049, China
[†]These authors contributed equally to this work.
*Correspondence address. Tel: +86-18966728272; E-mail: gzk@nwafu.edu.cn

Received 5 August 2021 Accepted 7 December 2021

Abstract

The gene dosage at the imprinted *Dlk1-Dio3* locus is critical for cell growth and development. A relatively high gene expression within the *Dlk1-Dio3* region, especially the active expression of *Gtl2*, has been identified as the only reliable marker for cell pluripotency. The DNA methylation state of the IG-DNA methylated regions (DMR), which is located upstream of the *Gtl2* gene, dominantly contributes to the control of gene expression in the *Dlk1-Dio3* locus. However, the precise mechanism underlying the regulation of DNA methylation in the IG-DMR remains largely unknown. Here, we use the F9 embryonal carcinoma cell line, a low pluripotent cell model, to identify the mechanism responsible for DNA methylation in the IG-DMR, and find that the interaction of PGC7 with UHRF1 is involved in maintaining DNA methylation and inducing DNA hypermethylation in the IG-DMR region. PGC7 and UHRF1 cooperatively bind in the IG-DMR to regulate the methylation of DNA and histones in this imprinted region. PGC7 promotes the recruitment of DNMT1 by UHRF1 to maintain DNA methylation in the IG-DMR locus. The interaction between PGC7 and UHRF1 strengthens their binding to H3K9me3 and leads to further enrichment of H3K9me3 in the IG-DMR by recruiting the specific histone methyltransferase SETDB1. Consequently, the abundance of H3K9me3 promotes DNMT3A to bind to the IG-DMR and increases DNA methylation level in this region. In summary, we propose a new mechanism of DNA methylation regulation in the IG-DMR locus and provide further insight into the understanding of the difference in *Gtl2* expression levels between high and low pluripotent cells.

Key words PGC7, UHRF1, IG-DMR, DNA methylation, H3K9me3

Introduction

The delta-like non-canonical Notch ligand 1/iodothyronine deiodinase 3 (*Dlk1-Dio3*) imprinted region is located on the mouse chromosome 12 (12F1) and the human chromosome 14q32. It contains three protein-coding genes, *Dlk1*, *Rtl1*, and *Dio3*, expressed from the paternally inherited chromosome and multiple long and small noncoding RNA (ncRNA) genes expressed from the maternally inherited chromosome. The expression levels of the imprinted genes in this locus regulate cell development and growth. Alterations of the imprinted gene dosage in the *Dlk1-Dio3* region cause multiple phenotypes including growth deficiencies and developmental defects of embryos and placenta, as well as defects in adult metabolism and brain function. Within the *Dlk1-Dio3* region, the imprinting regulation requires two different DNA methylated regions (DMRs), the intergenic-DMR (IG-DMR) and the gene-trap line 2-DMR (*Gtl2*-DMR) [1,2]. The DNA methylation state in the IG-DMR is not only essential for proper imprinting control but also relevant for the imprinted gene dosage. Therefore, understanding the regulation of DNA methylation in this region may have implications for human disorders such as cancer and be useful for basic and medical research. Importantly, *Gtl2*, one of the long ncRNAs (lncRNAs) located in the *Dlk1-Dio3* region, was reported to be a tumor suppressor [3]. A decreased *Gtl2* expression level is considered as a biomarker for various cancer prognosis and diagnosis [4].

Recently, it was reported that the expression of imprinted genes in the *Dlk1-Dio3* region is critical to maintain stem cell pluripotency.

Particularly, *Gtl2* expression level is considered as the only reliable marker to distinguish low-grade from high-grade induced pluripotent stem cells (iPSCs) [5–7]. Pluripotency genes regulate lncRNAs derived from the *Dlk1-Dio3* region to maintain the pluripotency of mouse embryonic stem cells (mESCs) [8,9]. For example, *Gtl2* modulates the expression levels of pluripotency genes [10], which in turn regulate the methylation of lncRNA promoters and affect lncRNA expression in cells [9,11,12]. Moreover, silencing of the imprinted *Dlk1-Dio3* gene cluster induced by DNA hypermethylation in the IG-DMR was observed in most iPSC clones that contributed poorly to chimeras and failed to support the development of iPSC-derived animals [7,13,14]. However, the cause of IG-DMR hypermethylation in low-grade iPSCs remains unclear. Here, we used F9 embryonal carcinoma (EC) cells, a partially pluripotent cell line in which the IG-DMR is hypermethylated with a low expression level of *Gtl2*, to identify the mechanism responsible for DNA methylation in the IG-DMR.

The primordial germ cell 7 (PGC7) protein comprises 150 amino acids and is encoded by a maternal effect gene that is specifically expressed in primordial germ cells, oocytes, and pluripotent cells [15]. In zygotes, PGC7 binds to H3K9me2 in the female pronucleus to protect the maternal genome from the Tet methylcytosine dioxygenase3 (TET3)-mediated active demethylation process [16]. In iPSC reprogramming, exogenous PGC7 efficiently improves the reprogramming fidelity with a higher proportion of high-grade iPSCs through maintaining the imprinting of the IG-DMR at the *Dlk1-Dio3* locus by suppressing DNMT3A enrichment [17]. In pluripotent cells, PGC7 plays a significant role in the maintenance of a naïve pluripotency state [18]. High PGC7 level corresponds to more active histone modifications and low DNA methylation, whereas low PGC7 level correlates with high levels of repressive histone modifications and DNA methylation [19]. Previously, we predicted that PGC7 is an intrinsically disordered protein (IDP), which might adopt various protein conformations that varies from protein-protein interactions. Therefore, we speculated that different functions of PGC7 in different cells might depend on different protein interaction partners, different biological contexts, or even both [20].

Ubiquitin-like with plant homeodomain and ring finger domains 1 (UHRF1), a PGC7 interaction partner, is an oncogene that is essential for the maintenance of DNA methylation [21,22]. UHRF1 contains five major protein domains: an ubiquitin-like (UBL) domain, a tandem Tudor domain (TTD), a plant homeodomain (PHD) finger, a SET and RING associated (SRA) domain, and a really interesting new gene (RING) finger [6,23,24]. UHRF1 recognizes hemimethylated CG sites through its SRA domain. The E3 ubiquitin ligase activity of UHRF1 RING finger promotes the ubiquitination of H3K18 and H3K23, which recruits DNMT1 for the methylation of the unmodified C of hemimethylated CG sites to copy the existing methylation patterns [25,26]. In addition, the TTD and PHD finger might contribute to the proper localization of UHRF1 through recognizing H3K9me2/3 and unmodified H3R2, respectively [27]. In cancer cells, UHRF1 acts by silencing tumor suppressors (including *Gtl2*) through a DNA methylation-dependent mechanism [28]. Due to the interaction of PGC7 with UHRF1 and their binding to methylated H3K9, we speculated that PGC7 and UHRF1 might co-localize in the IG-DMR and participate in the regulation of DNA methylation at imprinted loci.

In the present study, we find that PGC7 and UHRF1 are cooperatively associated with the IG-DMR in F9 EC cells. PGC7 promotes UHRF1-mediated recruitment of DNMT1 and SETDB1, both of which engage in DNA methylation maintenance and H3K9me3 enrichment. Subsequently, DNMT3A recognizes H3K9me3 and results in DNA hypermethylation in the IG-DMR of the *Dlk1-Dio3* region. We uncover a mechanism possibly occurring in tumor cells, primed-state pluripotent stem cells, and low-grade iPSCs, in which the IG-DMR is hypermethylated and the pluripotency marker *Gtl2* is repressed.

Materials and Methods

Cell culture and transfection

HEK-293T cells and F9 embryonal carcinoma (EC) cells were obtained from the American Type Culture Collection (ATCC, Manassas, USA) and cultured in Dulbecco's modified Eagle's medium (DMEM) supplemented with 10% (v/v) FBS in the sterile cell wells which were purchased from Nunclon (Roskilde, Denmark). All cells were maintained at 37°C and 5% CO_2 in a humidified incubator.

Transfections were performed by using Lipofectamine 2000 (Life Technologies, Carlsbad, USA) according to the manufacturer's instructions. All cell culture reagents were purchased from Gibco (Carlsbad, USA) unless indicated.

Construction of plasmids

The full-length coding sequences of the *Uhrf1* and *Pgc7* were amplified from cDNA of F9 ECs, then these sequences were constructed into pCMV-HA and p3 × Flag-CMV-10 or pCMV-Myc plasmids by standard molecular cloning methods and confirmed by sequencing. The coding sequence of *Dnmt1* was constructed into p3 × Flag-CMV-10 plasmid, and *Dnmt3a* was constructed into p3 × Flag-CMV-10 plasmid. The fused coding sequence of *Uhrf1* and *Pgc7* was constructed into pCMV-HA plasmid and the T2A peptide was used as the linker between respective coding sequence of *Uhrf1* and *Pgc7*. All the primers used for construction of the above plasmids are listed in Supplementary Table S1.

RNA interference

Short interfering RNAs (siRNAs) that target mouse *Pgc7*, *Uhrf1*, *Setdb1* and negative control siRNA-NC were purchased from Shanghai GenePharma (Shanghai, China). siRNAs sequences are as follows: si-Pgc7, 5′-GCACAACGAUCCAGAUUUA-3′; si-Uhrf1, 5′-GUGGUCAUGGCCAACUAUATT-3′; si-Setdb1, 5′-GCUACAUCAUUGAUGCCAAACUUGA-3′; siRNA-NC, 5′-UUCUCCGAACGUGUCACGUTT-3′. For RNA interference experiments, F9 ECs were transfected with the indicated siRNAs (50 nM final concentration) using Lipofectamine 2000.

Reverse transcription PCR and quantitative real-time PCR analysis

Total RNA was extracted from treated cells using Trizol Reagent (Life Technologies) according to the manufacturer's protocol. Total RNA (1 μg) was reverse-transcribed using a PrimeScript RT reagents kit (TaKaRa, Dalian, China) with the following protocol: reactions were carried out at 37°C for 15 min and 85°C for 5 s. The amount of RNA was determined by real-time PCR on an ABI StepOnePlus PCR system (Applied Biosystems, Foster City, USA) using SYBR Premix Ex Taq II (TaKaRa). The following conditions were used for qPCR: 30 s at 95°C, and 40 cycles of 5 s at 95°C and 30 s at 60°C, and the melting curve was analyzed to ensure that a single PCR product was obtained. Data were collected after each annealing

step. Glyceraldehyde-3-phosphate dehydrogenase (*GAPDH*) was used as an endogenous control to normalize for the differences in the amount of total RNA in each sample. All primer sequences used for qPCR examination were obtained from the PrimerBank (http://pga.mgh.harvard.edu/primerbank/) and shown in the Table 1.

Co-immunoprecipitation

After 48 h, the transfected F9 ECs were washed with PBS twice and lysed in ice-cold Pierce IP lysis buffer (Pierce, Rockford, USA) supplemented with proteinase inhibitor cocktail (Thermo Scientific, Waltham, USA). Cleared cell lysates (0.5 mL) were pre-incubated with Pierce™ Protein A/G Magnetic Agarose Beads (Thermo Scientific) for 1 h at 4°C to reduce non-specific binding of proteins to the beads. After brief spin, the pre-cleared cell lysates were incubated with 2 μg of indicated antibodies overnight at 4°C, and the lysates were added in Pierce™ Protein A/G Magnetic Agarose Beads and incubated for 3 h. Then the immunoprecipitates were analyzed by western blot analysis. The biotin co-immunoprecipitation was preformed using bio-peptides of H3, H3K9me2 and H3K9me3 in HEK-293T cells with overexpression of PGC7 and UHRF1, the Streptavidin Dynabeads™ M-280 were used to pull down the complex that bio-peptides bound to. The information bio-peptides is as follows: L-H3, biotin-ARTKQTARKSTGGKAPRKQLA; L-H3K9me2, biotin-ARTKQTARK(me2)STGGKAPRKQLA; L-H3K9me3, biotin-ARTKQTARK(me3)STGGKAPRKQLA.

Table 1. Sequences of the primers used for qPCR analysis

Gene name	Primer sequences (5′→3′)	
GAPDH	Forward	TGTGAGGGAGATGCTCAGTG
	Reverse	TGTTCCTACCCCCAATGTGT
Nanog	Forward	CACCCACCCATGCTAGTCTT
	Reverse	ACCCTCAAACTCCTGGTCCT
Klf4	Forward	GGCGAGTCTGACATGGCTG
	Reverse	GCTGGACGCAGTGTCTTCTC
Oct4	Forward	TAGGTGAGCCGTCTTTCCAC
	Reverse	GCTTAGCCAGGTTCGAGGAT
Sox2	Forward	CTGGACTGCGAACTGGAGAA
	Reverse	CTAGTCGGCATCACGGTTTT
Klf2	Forward	CTCAGCGAGCCTATCTTGCC
	Reverse	CACGTTGTTTAGGTCCTCATCC
Esrrb	Forward	GCACCTGGGCTCTAGTTGC
	Reverse	TACAGTCCTCGTAGCTCTTGC
H19	Forward	TTGCACTAAGTCGATTGCACT
	Reverse	GGAACTGCTTCCAGACTAGGC
Rasgrf1	Forward	GCCAGAAGACTTGACAACGCT
	Reverse	TCAATCTACAGGGATGGTGGAAG
Gtl2	Forward	TCCTCACCTCCAATTTCCCCT
	Reverse	GAGCGAGAGCCGTTCGATG
P1	Forward	TTTACCGTGGCACAGATTCA
	Reverse	CTGTGAGGCACTTGGCCTAT
P2	Forward	CACAGCAAAAGTGCATGGAT
	Reverse	CCATGGCACAACTACACAGG
P3	Forward	TCCCATACCAAGCACAATGA
	Reverse	GTCCACAGCACATCTCCGTA
P4	Forward	GCTTTGGAATTCCTGATGGA
	Reverse	GGCTACAGCAGGGAGACAAG

Alkaline phosphatase (AP) staining

Cytochemical staining for AP was performed using the Alkaline Phosphatase Kit (C3206; Beyotime Biotechnology, Shanghai, China) according to the manufacturer's protocol.

Immunofluorescence microscopy

F9 ECs were fixed with 4% paraformaldehyde/PBS for 20 min, permeabilized with 0.2% Triton X-100/PBS for 10 min, and rinsed twice in PBS. Cells were incubated with the indicated primary antibodies diluted in blocking buffer (Beyotime) overnight at 4°C and washed three times (5 min each) with washing buffer (Beyotime), followed by incubation with an Alexa Fluor 488/555-conjugated secondary antibody for 2 h at room temperature. The cell nuclei were counterstained with DAPI. Finally, cells were examined with a fluorescence microscope.

Western blot analysis

Cells were lysed with RIPA buffer (Pierce). BCA Protein Assay Reagent (Pierce) was used to determine the protein concentration of lysate. Equal amounts of protein were resolved by 8% ~ 12% SDS-PAGE. Then the proteins were transferred to the polyvinylidene fluoride membranes (Millipore, Billerica, USA). After being blocked for 2 h at room temperature in 10% nonfat dry milk in TBST containing 0.05% Tween-20, the membranes were incubated with primary antibodies overnight at 4°C and washed with TBST. Then membranes were incubated with HRP-conjugated secondary antibodies for 2 h at room temperature. Primary antibodies included rabbit anti-Flag (1:1000; Thermo Scientific), rabbit monoclonal anti-GAPDH and mouse anti-HA (1:5000; Sigma, St Louis, USA), rabbit anti-H3K9me2 and rabbit anti-H3K9me3 (CST, Danvers, USA), mouse anti-antibody-H3 (1:1000; Sangon Biotech, Shanghai, China), rabbit Polyclonal anti-Setdb1, rabbit Polyclonal anti-Oct4 (1:1000; Proteintech, Rosemont, USA). The horseradish peroxidase (HRP)-conjugated anti-rabbit/mouse IgG secondary antibodies were obtained from Beyotime Institute of Biotechnology (Shanghai, China).

Chromatin Immunoprecipitation

F9 ECs were cultured to a density of 1×10^8 cells for each immunoprecipitation experiment. Cells were cross-linked for 10 min at room temperature with 1% (w/v) formaldehyde and the reaction was subsequently quenched with 125 mM glycine. Genomic DNA was isolated and sheared to average lengths of 300 ~ 500 bp by micrococcal nuclease and ultrasonic treatment. Then, specific antibodies were used for immunoprecipitation. Chromatin immunoprecipitation (ChIP) enrichment was purified using the QIAEX II Gel Extraction Kit (Qiagen, Germantown, USA), and the collected DNA was subject to qPCR. Fold-enrichment was determined by normalizing threshold cycle values of antibody ChIP against IgG ChIP. Primer sequences used for ChIP-qPCR are listed in Table 1.

Bisulfite sequence analysis

The DNAs of F9 cells with different treatments were bisulfite-treated using EZ DNA Methylation-Gold Kit (ZYMO Research, Irvine, USA). To amplify the DMRs of IG-DMR, fully or seminested PCR was performed using DNA polymerase ExTaq HS (Takara). The first

round of PCR consisted of the following cycle conditions: 2 min at 94°C for 1 cycle and 30 s at 94°C, 30 s at 50°C and 1 min at 68°C for 33 cycles. The second round of PCR consisted of the following cycle conditions: 2 min at 94°C for 1 cycle and 30 s at 94°C, 30 s at 55°C and 1 min at 72°C for 33 cycles. Primer sequences used for bisulfite sequence analysis are listed in Supplementary Table S2. The products were purified using the QIAEX II Gel Extraction Kit (Qiagen), and cloned into the pGEM-19T Vector (Promega, Madison, USA) and were sequenced by AuGCT company (Xi'an, China).

Statistical analysis

Data were expressed as the mean ± SD. The difference between two groups was compared by a two-tailed paired Student's *t*-test, and significance was set at $P < 0.05$. The difference among three or more groups was compared by an analysis of variance (ANOVA), and significance of difference was determined by post hoc testing.

Results

The interaction between PGC7 and UHRF1 contributes to their subcellular co-localization and the pluripotency regulation

Previous studies from our laboratory and Funaki et al. have reported the interaction between PGC7 and UHRF1 [20,29]. This observation was reconfirmed by co-immunoprecipitation (co-IP) experiments (Figure 1A). Furthermore, we constructed a series of truncated mutants of UHRF1 or PGC7 to map PGC7 and UHRF1 regions involved in the interaction. Figure 1B,C showed that PGC7 N-terminus interacted with the UHRF1 first low complexity motif, located between UHRF1 PHD and SRA domains. Li *et al.* [30] showed that PGC7 promotes UHRF1 export from the nucleus in oocytes. Interestingly, our results in F9 ECs are significantly different from those obtained using oocytes. Immunofluorescence analyses (Supplementary Figure S1) showed more localization of PGC7 in the cytoplasm than that in the nucleus, whereas UHRF1 tended to be distributed in the nucleus rather than in the cytoplasm. When being co-transfected into cells with *UHRF1*, PGC7 relocated to the nucleus, whereas the distribution of UHRF1 was not affected. Notably, the co-localization of PGC7 and UHRF1 was confined to specific areas within the nucleus, suggesting that they might work together at specific genomic loci.

We predicted that PGC7 is an IDP without specific functions due to the lack of defined conformation. We also speculated that PGC7 mainly regulates the function of its binding partners through protein interactions. It is well known that ESCs should be cultured in a leukemia inhibitory factor (LIF)-containing medium to maintain the cell pluripotency. Recently, the 2i culture method, which uses a combination of mitogen-activated protein kinase kinase inhibition (MEKi) and glycogen synthase kinase 3 inhibition (GSK3i), was developed to maintain ESCs in the naïve state. Both methods differentially prevent cells from differentiating. It was reported that decreased UHRF1 expression is the main cause of global demethylation under 2i culture conditions that induces transition of mESCs from the primed to the naïve state, suggesting that UHRF1-mediated maintenance of DNA methylation is not conducive to DNA hypomethylation which exists in pluripotent cells [31,32]. Hence, we further investigated whether PGC7 is involved in regulating UHRF1 functions in cell pluripotency and DNA methylation. The alkaline phosphatase (AP) staining assay is used to distinguish differentiated cells from cells in naïve state. Although most cell types produce AP, pluripotent cells show significantly more staining than other cell types [33–35]. We used that characteristic to determine the pluripotency of F9 ECs. Knockdown of *Uhrf1* with small interference RNA (siRNA) significantly promoted AP staining in F9 ECs, whereas knockdown of *Pgc7* had no obvious effect. Simultaneous knockdown of *Pgc7* and *Uhrf1* did not significantly change the AP staining obtained upon *Uhrf1* single knockdown (Figure 1D,E). A similar result was obtained for the global DNA demethylation induced by *Uhrf1* depletion (Figure 1G,H). In order to further confirm the effect of PGC7 and UHRF1 in cell pluripotency, the expressions of pluripotency transcription factors OCT4 were tested by western blot analysis. The protein expression of OCT4 was up-regulated in individual knockdown of *Uhrf1* or simultaneous knockdown of *Uhrf1* and *Pgc7*, whereas it was down-regulated in individual knockdown of *Pgc7* (Figure 1F). These results indicated that the interaction between PGC7 and UHRF1 did not modulate the effect of UHRF1 on maintaining global DNA methylation and antagonizing cell pluripotency. Subsequently, we investigated the regulatory effects of PGC7 and UHRF1 on the expressions of candidate pluripotency and imprinted genes. Ectopic overexpression of UHRF1 but not PGC7 significantly repressed the transcription of pluripotency genes except *Nanog*. Only the UHRF1-triggered downregulation of *Gtl2* was enhanced by co-expression with PGC7 (Figure 1I). Knockdown of both *Pgc7* and *Uhrf1* further promoted the expression of *Gtl2* compared to the expression observed after *Uhrf1* individual knockdown (Figure 1K). The overexpression or silencing efficiencies of *Pgc7 and Uhrf1* were examined by western blot analysis (Figure 1J,L). Collectively, these results supported our previous speculation that PGC7 and UHRF1 have synergistic effects at specific sites in the genome and suggested that the *Dlk1-Dio3*-imprinted locus is such a site.

UHRF1 and PGC7 cooperatively bind to the IG-DMR and induce DNA hypermethylation

The IG-DMR is located upstream of *Gtl2* in the Dlk1-Dio3 region and was reported to be an enhancer involved in Gtl2 regulation, which depends on its DNA methylation status. Given that PGC7 binds to the IG-DMR to maintain imprinting, we speculated that the interaction between PGC7 and UHRF1 may play a role in this region to regulate Gtl2 expression. To verify this hypothesis, chromatin immunoprecipitation-quantitative real-time polymerase chain reaction (CHIP-qPCR) assays was performed using the primers for P1 to P5 sites surrounding the PGC7 binding sites in the IG-DMR (Figure 2A) [17]. The results showed that PGC7 and UHRF1 exclusively bound to P3 but not to other sites, represented by P4 site (Supplementary Figure S2). In addition, when being co-transfected into cells, PGC7 and UHRF1 promoted each other's enrichment at the P3 site (Figure 2B,C). These results indicated that PGC7 and UHRF1 had synergistic effects on their binding to the IG-DMR. This was further confirmed by the ChIP-qPCR results which showed that the downregulation of one by siRNA inhibited the enrichment of the other at the P3 site in IG-DMR (Figure 2D,E). Therefore, the co-localization of PGC7 and UHRF1 in the IG-DMR depends on their interaction.

To test whether the interaction between PGC7 and UHRF1 is involved in the regulation of DNA methylation in the IG-DMR, we assessed DNA methylation in the binding region of UHRF1 and PGC7 by methylated DNA immunoprecipitation (Me-DIP) assay. The results revealed that 5-methylcytosine (5-mC) was enriched more at the P3 site than at the surrounding sites P2 and P4, whereas

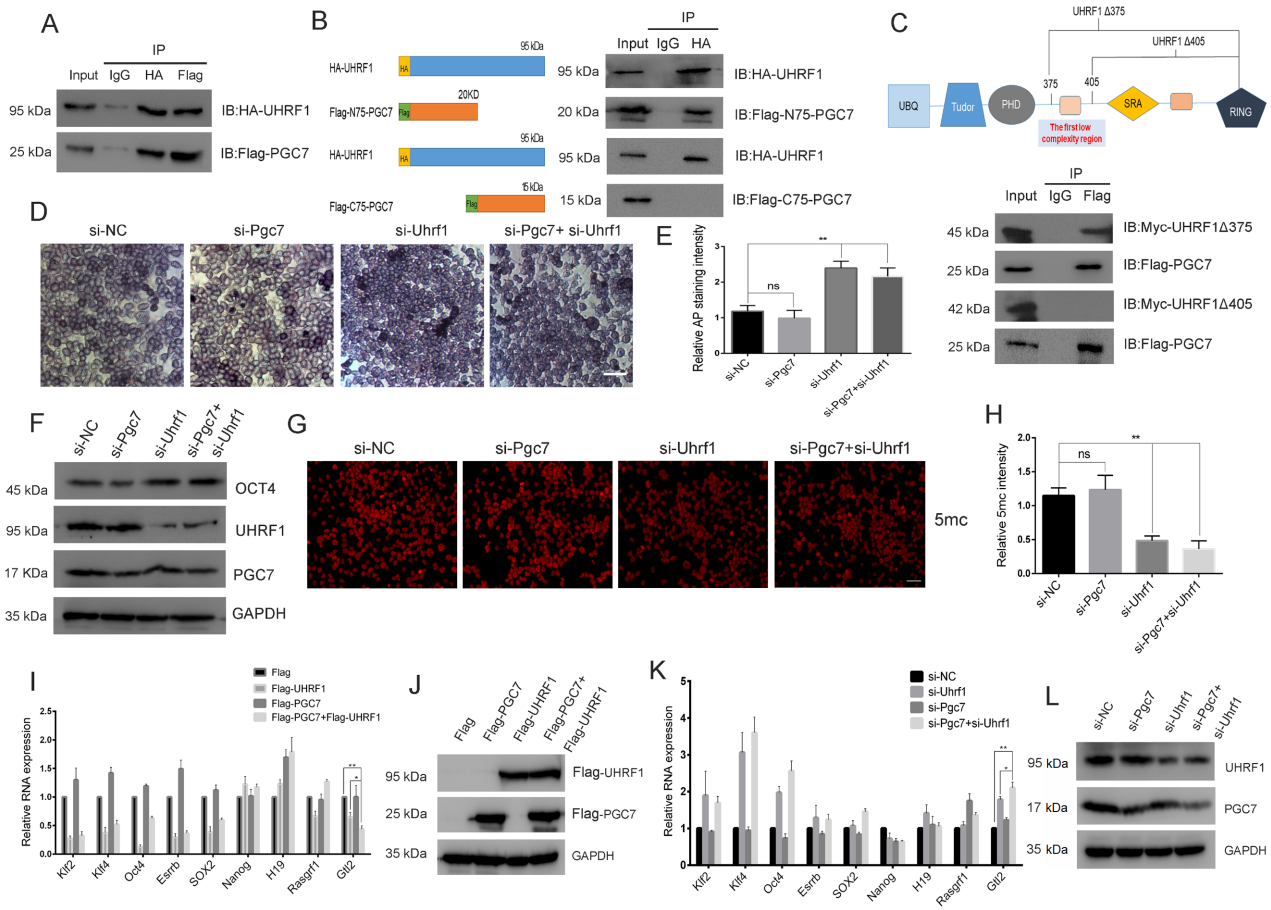

Figure 1. The interaction between PGC7 and UHRF1 contributes to their subcellular colocalization and the regulation of pluripotency (A) PGC7 interacted with UHRF1 in HEK-293T cells. HEK-293T cells were transfected with pCMV-HA-UHRF1 and pCMV-Flag-PGC7. Antibodies recognizing the Flag tag or the HA tag were used to capture N-Flag-tagged protein-PGC7 complexes or N-HA-tagged protein-UHRF1 complexes, respectively, for co-immunoprecipitation. Normal mouse IgG served as negative control. (B) The N-terminus of PGC7 interacted with UHRF1. pCMV-HA-UHRF1 was co-transfected with pCMV-Flag-N75-PGC7 or pCMV-Flag-C75-PGC7 into HEK-293T cells. The anti-HA tag antibody was used to capture N-HA-tagged protein-UHRF1 complexes. Normal mouse IgG served as negative control. (C) PGC7 was associated with the first low complexity of UHRF1 in HEK-293T cells. pCMV-HA-UHRF1Δ375 or pCMV-HA-UHRF1Δ405 was co-transfected with pCMV-Flag-PGC7 into HEK-293T cells. Anti-Flag tag antibody was used to capture N-Flag-tagged protein-PGC7 complexes. Normal mouse IgG served as negative control. (D,E) AP staining upon different treatments of F9 ECs. The NC-siRNA, *Pgc7*-siRNA, *Uhrf1*-siRNA, or both *Pgc7*-siRNA and *Uhrf1*-siRNA were transfected into F9 EC cells. AP staining assay was performed 36 h after transfection, and the AP staining intensity was measured using the ImageJ software. At least three images were analyzed for each treatment and the experiment was performed four times. Scale bar = 20 μm. (F) The expression of pluripotency transcription factor OCT4 was tested by western blot analysis. F9 EC cells were transfected as indicated and cultured for following 36 h. (G,H) DNA demethylation was analyzed by 5mC staining. F9 EC cells were transfected as indicated and cultured for following 36 h. Afterward, 5mC was stained and the fluorescence intensity was measured with the Image J software. At least three images were analyzed for each treatment and the experiment was performed four times. Scale bar = 50 μm. (I,K) Some pluripotency-related genes including *Gtl2* were regulated by UHRF1 or PGC7. The F9 ECs were transfected as indicated. 36 h after transfection, the pluripotency-related genes were analyzed by RT-qPCR. (J,L) The overexpression or silencing efficiencies of *Pgc7* and *Uhrf1* were examined by western blot analysis.

there was no enrichment at P1 (Figure 2F). This suggested that the co-localization between PGC7 and UHRF1 is involved in DNA methylation in the IG-DMR. Subsequently, bisulfite sequencing assays were performed to analyze DNA methylation at the P3 site. Suppressing either PGC7 or UHRF1 led to DNA demethylation in the IG-DMR and knockdown of both resulted in more significant demethylation (Figure 2G), suggesting that the interaction between PGC7 and UHRF1 facilitates the maintenance of DNA methylation in the IG-DMR. Additionally, overexpression of either PGC7 or UHRF1 only slightly increased DNA methylation in the IG-DMR, whereas concurrent overexpression of both significantly enhanced the methylation level of the IG-DMR (Figure 2H). These results indicated that the interaction between PGC7 and UHRF1 in the IG-DMR contributes not only to DNA methylation maintenance, but also to DNA hypermethylation.

UHRF1, unlike PGC7, directly contributes to DNMT1 recruitment to maintain DNA methylation in the IG-DMR

The SRA domain of UHRF1 recruits DNMT1 to methylate the hemimethylated CG sites generated by the DNA replication process [25]. We wondered whether PGC7 is involved in regulating the recruitment of DNMT1 to the IG-DMR mediated by UHRF1. Co-IP assays revealed that PGC7 does not interact with DNMT1 directly, whereas UHRF1 does (Figure 3A). Interestingly, when being co-expressed with myc-UHRF1, PGC7 could be co-immunoprecipitated with DNMT1, suggesting that UHRF1, PGC7, and DNMT1 exist in a complex with UHRF1, which is an intermediate bridge between PGC7 and DNMT1 (Figure 3B). It was reported that PGC7 induces the ex-

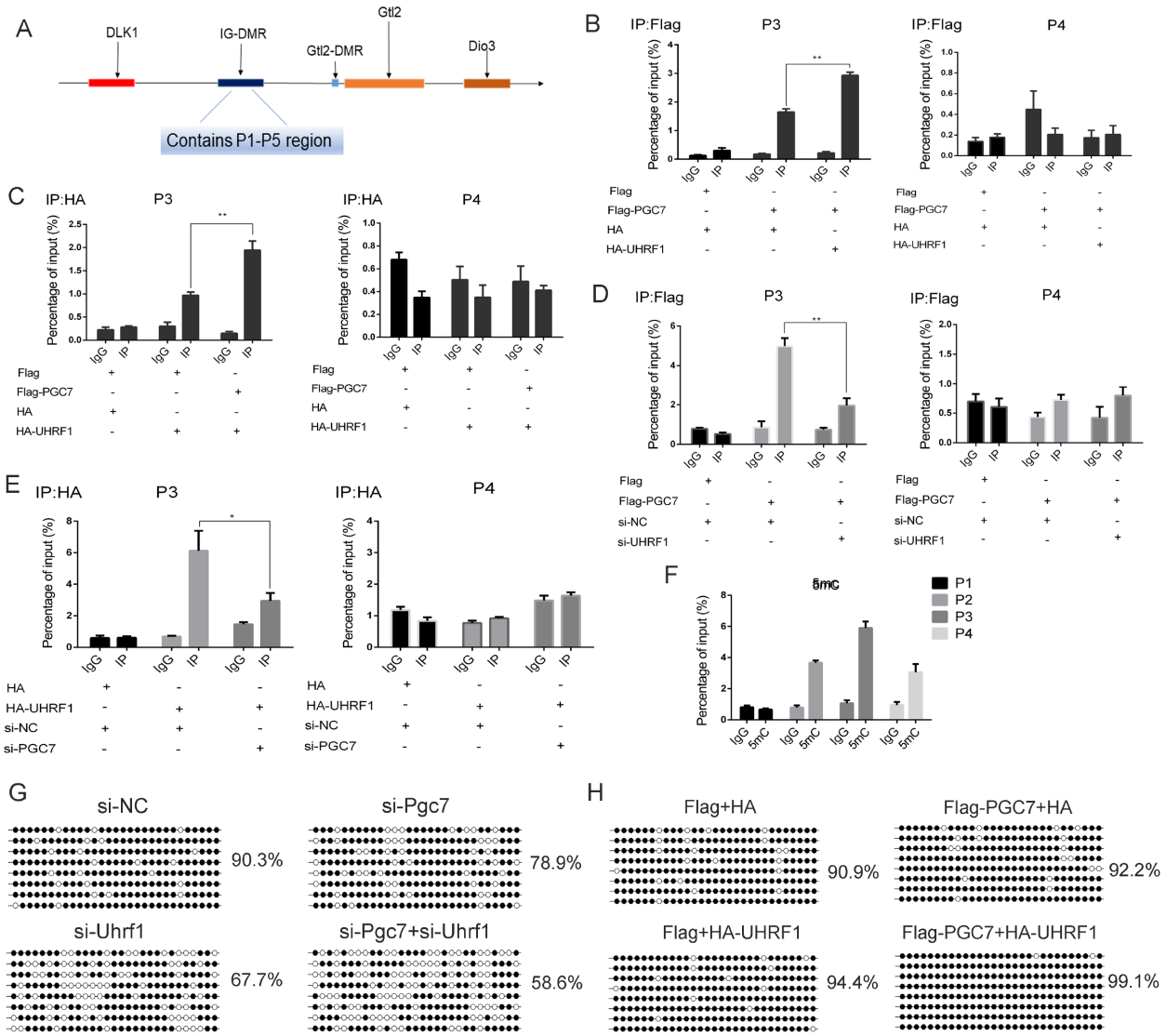

Figure 2. UHRF1 and PGC7 cooperatively bind to the IG-DMR and induce DNA hypermethylation (A) The abridged general view of *Dlk1-Dio3* region. (B,C) PGC7 or UHRF1 was enriched in IG-DMR, which was further enhanced by interaction between PGC7 and UHRF1. P3 but not P4 was the specific PGC7 binding site in *Dlk1-Dio3* region. The F9 ECs were transfected as indicated. And 48h after transfection, ChIP assay was performed using anti-Flag tag (B) or anti-HA tag (C) antibody. Normal mouse IgG served as the negative control. (D,E) PGC7 and UHRF1 had synergistic effects on their binding to the P3. The F9 ECs were transfected with plasmids and siRNAs as indicated. 48h after transfection, ChIP assay was performed using anti-Flag tag (D) or anti-HA tag (E) antibody. Normal mouse IgG served as the negative control. (F) 5mC was enriched in multiple regions in *Dlk1-Dio3* imprinted loci. ChIP assays were performed using anti-5mC antibody in F9 ECs. Normal mouse IgG served as the negative control. (G,H) Methylation levels of IG-DMR with siRNA (G) or plasmids (H) transfection. And 48 h after transfection, F9 ECs were collected to purify DNA. Bisulfite sequencing assay was performed to analyze the methylation level of different treatment groups.

tranuclear localization of UHRF1 and DNMT1 in oocytes [30]. Thus, we investigated whether PGC7 and UHRF1 affects the subcellular localization of DNMT1 in F9 ECs. The simultaneous overexpression of PGC7 and UHRF1 did not affect the nuclear localization of DNMT1, as shown in Supplementary Figure S3. Altogether, these results suggested that PGC7, UHRF1, and DNMT1 work together in F9 ECs.

To determine whether DNMT1 is involved in DNA methylation at the IG-DMR, ChIP-qPCR assays were performed. It was found that DNMT1 was specifically enriched at the P3 site in the IG-DMR (Figure 3C) and was co-localized with both PGC7 and UHRF1, as showed in Figure 2B,C. To verify that the recruitment of DNMT1 in the IG-DMR requires the interaction between PGC7 and UHRF1, ChIP-qPCR assays were performed after knockdown of endogenous *PGC7* or *UHRF1* using siRNAs. As showed in Figure 3D, UHRF1 knockdown completely disrupted DNMT1 enrichment at the P3 site, suggesting that UHRF1 is necessary for DNMT1 recruitment. PGC7 knockdown also led to a decreased DNMT1 recruitment (Figure 3E), which might be attributed to the reduced UHRF1 enrichment caused by PGC7 suppression. In summary, it is likely that the recruitment of DNMT1 is directly mediated by UHRF1, whereas the main role of PGC7 is to promote UHRF1 binding to the IG-DMR.

The interaction between PGC7 and UHRF1 promotes H3K9me3 enrichment in the IG-DMR

In addition to differential DNA methylation, the imprinted regions are associated with different histone modifications, which lead to

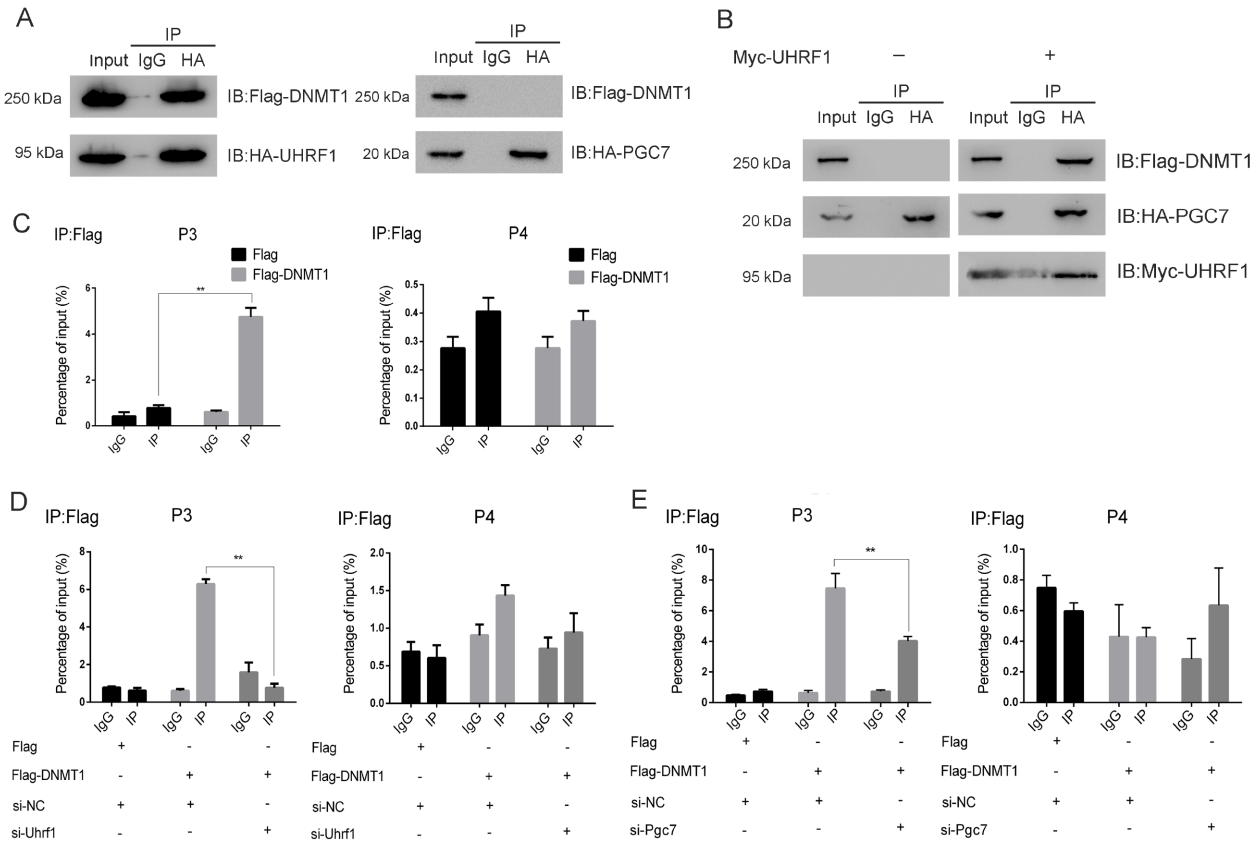

Figure 3. UHRF1, unlike PGC7, directly contributes to DNMT1 recruitment to maintain DNA methylation in the IG-DMR (A) UHRF1 but not PGC7 could recruit DNMT1 in HEK-293T cells. The HEK-293T cells were transfected with pCMV-Flag-DNMT1 and pCMV-HA-UHRF1, or pCMV-HA-PGC7 and pCMV-Flag-DNMT1, respectively. The anti-HA tag antibody was used to capture N-HA-tagged protein-PGC7 or protein-UHRF1 complexes. Normal mouse IgG served as the negative control. (B) PGC7 could recruit DNMT1 while UHRF1 was overexpressed in HEK-293T cells. The HEK-293T cells were transfected as indicated. The anti-HA antibody was used to capture N-HA-tagged protein-PGC7 complexes. Normal mouse IgG served as the negative control. (C) P3 but not P4 was the specific DNMT1 binding site. ChIP-qPCR analysis of Flag-tagged DNMT1 in F9 ECs. Primer P3 and P4 were used to detect whether DNMT1 could bind to IG-DMR. Normal mouse IgG served as the negative control. (D,E) UHRF1 and PGC7 were necessary for DNMT1 recruitment at P3. F9 ECs were transfected with pCMV-Flag-DNMT1 and *Uhrf1*-siRNA or *Pgc7*-siRNA as indicated. ChIP assays were performed using anti-Flag tag antibody. Primer P3 and P4 were used to detect the binding activity of DNMT1 to IG-DMR. Normal mouse IgG served as the negative control.

higher-order chromatin structures essential for imprinting maintenance and regulation of imprinted genes expression. Particularly, chromatin associated with the methylated alleles of imprinted regions is consistently marked by histone methylation [36]. Because the TTD domain of UHRF1 binds to H3K9me2/3 [37] and the N-terminus of PGC7 recognizes H3K9me2 for its nucleosome association, we wondered whether H3K9me2 facilitates the recruitment of the PGC7-UHRF1 complex. We synthesized three N-biotinylated peptides, containing 22 amino acids of the histone H3 N-terminal tail named L-H3, L-H3K9me2, and L-H3K9me3, representing unmethylated, demethylated, and trimethylated H3K9, respectively. As expected, the results of *in vitro* pulldown assays indicated that PGC7 has a tendency to associate with H3K9m2, whereas UHRF1 prefers H3K9me2/3. The interaction between PGC7 and UHRF1 not only enhanced their binding ability to histone H3, but also promoted the binding of PGC7 to H3K9me3 without changing the binding characteristics of UHRF1 (Figure 4A,B). These data suggested that PGC7 and UHRF1 co-localizes in nucleosomes with H3K9me3 modifications. This was confirmed by the ChIP-qPCR assays, which showed that H3K9me3 was enriched at the P3 site of the IG-DMR, which was co-localized with PGC7 and UHRF1, while H3K9me2 was enriched at the P4 site (Figure 4C). To further support our findings, we analyzed the ChIP-seq data from *Snyder et al.* (www.encodeproject.org/experiments/ENCSR000ADM/) using the *Roadmap* tool (http://epgg-test.wustl.edu/) and found that H3K9me3 modifications were enriched in the IG-DMR in E14 ESCs (Figure 4D).

We then investigated whether the enrichment of H3K9me3 in IG-DMR is related to the interaction between PGC7 and UHRF1. As shown in Figure 4E, individual knockdown of *Pgc7* or *Uhrf1* with siRNAs resulted in a slight decrease of H3K9me3 enrichment, whereas *Pgc7* and *Uhrf1* double knockdown significantly reduced H3K9me3 enrichment. In addition, the simultaneous, but not individual, overexpressing of PGC7 and UHRF1 significantly increased H3K9me3 enrichment in the IG-DMR (Figure 4F). Altogether, these results indicated that the interaction between PGC7 and UHRF1 promotes the enrichment of H3K9me3 in the IG-DMR. However, whether the enrichment of H3K9me3 is caused by the recruitment of the two factors or by enzymatic catalysis remains unclear. We detected the global H3K9me3 levels in cells with overexpression or knocking down *Pgc7* and *Uhrf1*. Although ectopic overexpression of UHRF1 only slightly increased H3K9me3 level and PGC7 overexpression had no effect, the concurrent over-

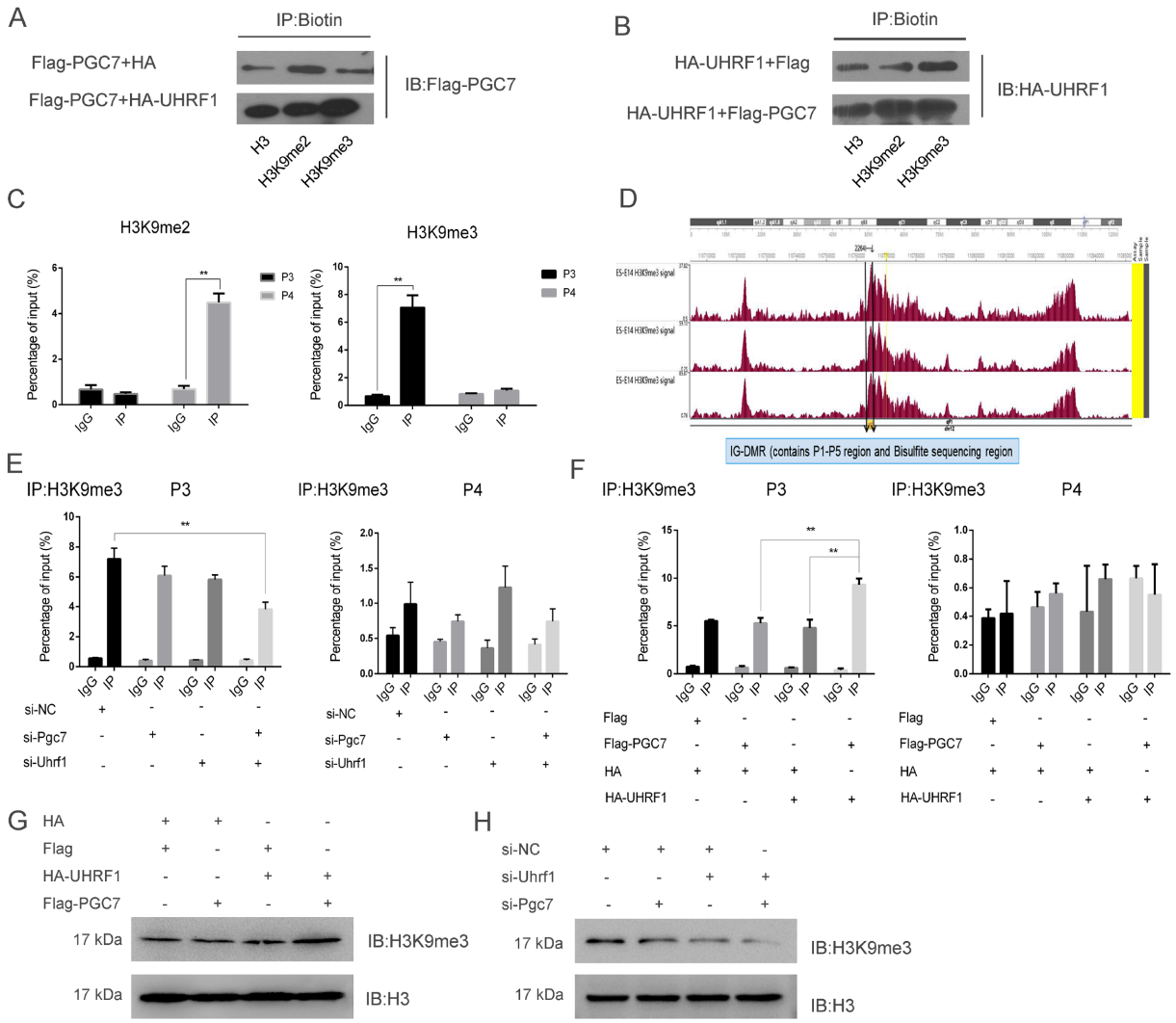

Figure 4. The interaction between PGC7 and UHRF1 promotes H3K9me3 enrichment in the IG-DMR (A,B) The interaction between PGC7 and UHRF1 promoted the binding of PGC7 to H3K9me3.HEK-293T cells were transfected with pCMV-HA, pCMV-Flag-PGC7 and pCMV-HA-UHRF1 (A) or pCMV-Flag, pCMV-Flag-PGC7 and pCMV-HA-UHRF1 (B). N-biotinylated peptides, containing 22 amino acids of histone H3 N-terminal, named H3, H3K9me2 and H3K9me3 were added into cell lysates. Streptavidin immunomagnetic beads were used to capture the complexes. (C) H3K9me3 was enriched at the P3 site. ChIP assay was performed using anti-H3K9me2 (Left) or anti-H3K9me3 (right) antibody in F9 ECs. Primer P3 and P4 were used to detect the enrichment of H3K9me2/3 at IG-DMR. Normal mouse IgG served as the negative control. (D) Information of histone imprinting of IG-DMR in E14 mouse embryonic stem cells from roadmap website. (E,F) The interaction between PGC7 and UHRF1 promotes the enrichment of H3K9me3 in the P3 site. F9 ECs were transfected with *Pgc7*-siRNA, *Uhrf1*-siRNA or both(E) or pCMV-HA, pCMV-HA-UHRF1, pCMV-Flag or pCMV-Flag-PGC (F) as indicated. ChIP assays were performed using anti-H3K9me3 antibody in F9 ECs. Primer P3 and P4 were used to detect the enrichment of H3K9me3 at IG-DMR. Normal mouse IgG served as the negative control. (G,H) PGC7 and UHRF1 might recruit H3K9 methyltransferase to methylate H3K9, which in turn leads to a further deposition of H3K9me3. F9 ECs were transfected with pCMV-HA, pCMV-HA-UHRF1, pCMV-Flag or pCMV-Flag-PGC7 (G), *Pgc7*-siRNA, *Uhrf1*-siRNA or both (H) as indicated. After 48 h, western blot analysis was preformed to detect the amount of H3K9me3. The H3 was used as an internal reference.

expression of UHRF1 and PGC7 significantly increased the intracellular H3K9me3 content (Figure 4G). Consistent with this, the individual knockdown of *Uhrf1*, but not of *Pgc7*, reduced the global level of H3K9me3, which were further decreased by *Uhrf1* and *Pgc7* double knockdown (Figure 4H). These results strongly indicated that, upon binding to the nucleosomes, PGC7 and UHRF1 might recruit H3K9 methyltransferase to methylate H3K9, which in turn leads to a further deposition of H3K9me3.

The recruitment of SETDB1 by UHRF1 is promoted by PGC7 and contributes to H3K9me3 enrichment

Two member of the H3K9 methyltransferase family, G9a (euchromatic histone-lysine N-methyltransferase 2, also known as EHMT2) and SETDB1 (SET domain, Bifurcated 1, also known as ESET and KMT1E), have been reported to be recruited by UHRF1 [38,39]. PGC7 disrupted the interaction between G9a and UHRF1 as shown by co-IP assays (Figure 5A), suggesting that the binding of PGC7 to UHRF1 does not facilitate G9a recruitment to the IG-DMR. This result is in line with our expectation, because G9a is responsible for H3K9 mono- and dimethylation, whereas SETDB1 leads mainly to H3K9 trimethylation [40]. As showed in Figure 5B,C, in addition to interacting with UHRF1, SETDB1 interacted with PGC7 in an UHRF1-independent manner. Interestingly, knockdown of PGC7 repressed the interaction between UHRF1 and SETDB1 (Figure 5D).

These results suggested that the recruitment of SETDB1 mediated by PGC7 and UHRF1 contributes to the global increase in H3K9me3 and H3K9me3 enrichment at the IG-DMR.

To verify this hypothesis, we performed ChIP-qPCR assay. SETDB1 specifically associated with the P3 site in the IG-DMR, and knockdown of either *Pgc7* or *Uhrf1* by siRNAs led to a decrease in SETDB1 enrichment (Figure 5E,F), suggesting that PGC7 and UHRF1 synergistically recruited SETDB1 to the IG-DMR. Interference with endogenous *Setdb1* expression reduced H3K9me3 global levels and up-regulated *Gtl2* expression in cells (Figure 5G,H). The enrichment of H3K9me3 in the IG-DMR was also reduced by decreased expression of endogenous *Setdb1* (Figure 5I), suggesting that SETDB1 contributes to H3K9me3 enrichment at the IG-DMR. Furthermore, bisulfite sequencing data indicated that knockdown of *Setdb1* resulted in a reduction of DNA methylation in the IG-DMR (Figure 5J), suggesting that the H3K9me3 enrichment induced by SETDB1 recruitment also participates in the regulation of DNA methylation in the IG-DMR.

H3K9me3 enrichment is required for UHRF1 to recruit DNMT3A

Methylated lysine residues in histone amino terminal tails can serve as docking sites for numerous proteins containing methyl-lysine-binding domains such as the chromodomain, PHD, or the Tudor domain (TD) [41]. To investigate whether the enrichment of

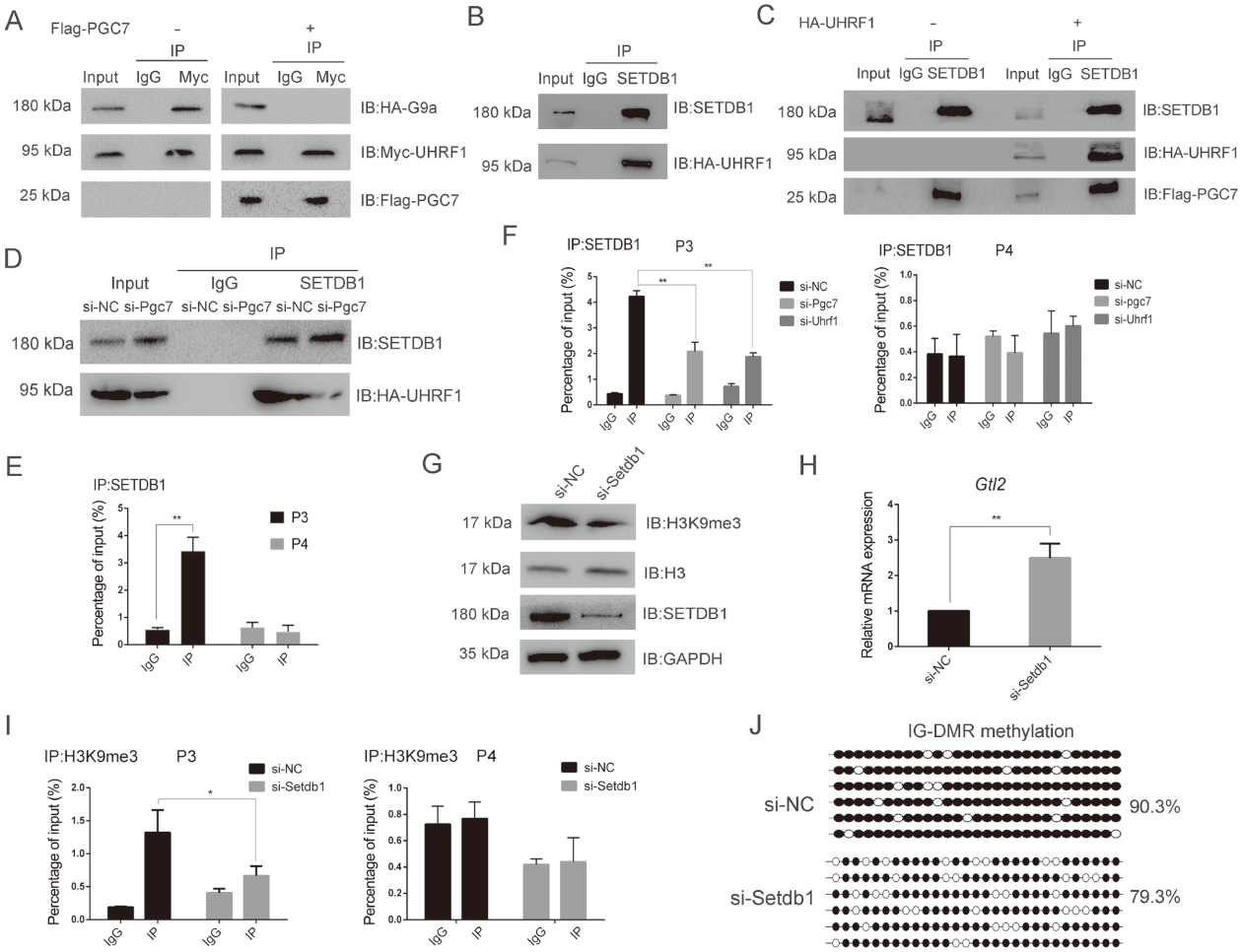

Figure 5. The recruitment of SETDB1 by UHRF1 is promoted by PGC7 and contributes to H3K9me3 enrichment (A) PGC7 intercepted the interaction between UHRF1 and G9A. The pCMV-Myc-UHRF1 and pCMV-Flag-PGC7 as well as pCMV-HA-G9A were transfected into HEK-293T cells. The anti-Myc antibody was used to capture N-Myc-tagged protein-UHRF1 complexes. Normal mouse IgG served as the negative control. (B) SETDB1 interacted with UHRF1 in F9 ECs. F9 ECs were transfected with pCMV-HA-UHRF1. The antibody for endogenous SETDB1 was used to capture protein-SETDB1 complexes. Normal mouse IgG served as the negative control. (C) UHRF1 promoted the interaction of SETDB1 with PGC7 in F9 ECs. The pCMV-HA-UHRF1 and pCMV-Flag-PGC7 were transfected into F9 ECs. The anti-SETDB1 antibody was used to capture protein-SETDB1 complexes. Normal mouse IgG served as the negative control. (D) The interference of PGC7 could impair the interaction between SETDB1 and UHRF1. The pCMV-HA-UHRF1 was transfected into F9 ECs. The anti-SETDB1 antibody was used to capture protein-SETDB1 complexes. Normal mouse IgG served as the negative control. (E, F) SETDB1 specifically associated with the P3 site in the IG-DMR, and knockdown of either *Pgc7* or *Uhrf1* by siRNAs led to a decrease in SETDB1 enrichment. ChIP assays were performed using anti-SETDB1 antibody. Primer P3 and P4 were used to detect the binding activity of SETDB1 to IG-DMR. Normal mouse IgG served as the negative control. (G, H) Interference with endogenous *Setdb1* expression reduced global H3K9me3 levels and up-regulated *Gtl2* expression. F9 ECs were transfected with *NC*-siRNA or *Setdb1*-siRNA as indicated. After 48 h, western blot analysis was preformed to detect the amount of H3K9me3 and SETDB1 (G). The expression of *Gtl2* was detected by RT-qPCR (H). (I) The enrichment of H3K9me3 in the IG-DMR was reduced by decreased expression of endogenous *Setdb1*. (J) Knockdown of *Setdb1* resulted in a reduction of DNA methylation in the IG-DMR. F9 ECs transfected with *Setdb1*-siRNA as indicated. 48h after transfection, F9 ECs were collected to purify DNA. Bisulfite sequencing assays were performed to analyze the methylation level of different treatment groups.

H3K9me3 in the IG-DMR favors the recruitment of UHRF1 and PGC7, we performed ChIP-qPCR assays of UHRF1 and PGC7 upon knockdown of endogenous *Setdb1*. As shown in Figure 6A, silencing of *Setdb1* did not significantly affect the enrichment of UHRF1 and PGC7 at the P3 site, suggesting that the resulting reduction of H3K9me3 did not influence the binding capacity of UHRF1 and PGC7 to the IG-DMR. The enrichment of the DNMT1 and the UHRF1-mediated recruitment of the maintenance DNA methyltransferase described above (Figure 3D,E) were not affected by the reduction of H3K9me3 in IG-DMR (Figure 6B). To further confirm this result, we added L-H3 and L-H3K9me3 to cell lysates containing recombinant Flag-DNMT1 and HA-UHRF1, and found that the interaction between DNMT1 and UHRF1 was improved by both L-H3 and L-H3K9me3 (Figure 6C). In parallel, reducing H3K9me3 level by knockdown of *Setdb1* did not alter the interaction between DNMT1 and UHRF1 (Figure 6D). Thus, these results suggested that UHRF1-mediated recruitment of DNMT1 depends only on the presence of the histone H3 N-terminus independently of H3K9 methylation state, which does not contribute to the recruitment of DNMT1 to maintain the normal imprinting of the IG-DMR.

It was reported that UHRF1 also recruits DNMT3A, a de novo DNA methyltransferase, to promote DNA methylation following H3K9 methylation [42]. To investigate whether the interaction between PGC7 and UHRF1 promotes DNMT3A recruitment, a co-IP assay was performed. As shown in Figure 6E, DNMT3A interacted with UHRF1 and PGC7, and the presence of PGC7 enhanced the association of DNMT3A with UHRF1 (Figure 6F). These results suggested that the interaction of UHRF1 with PGC7 facilitates the

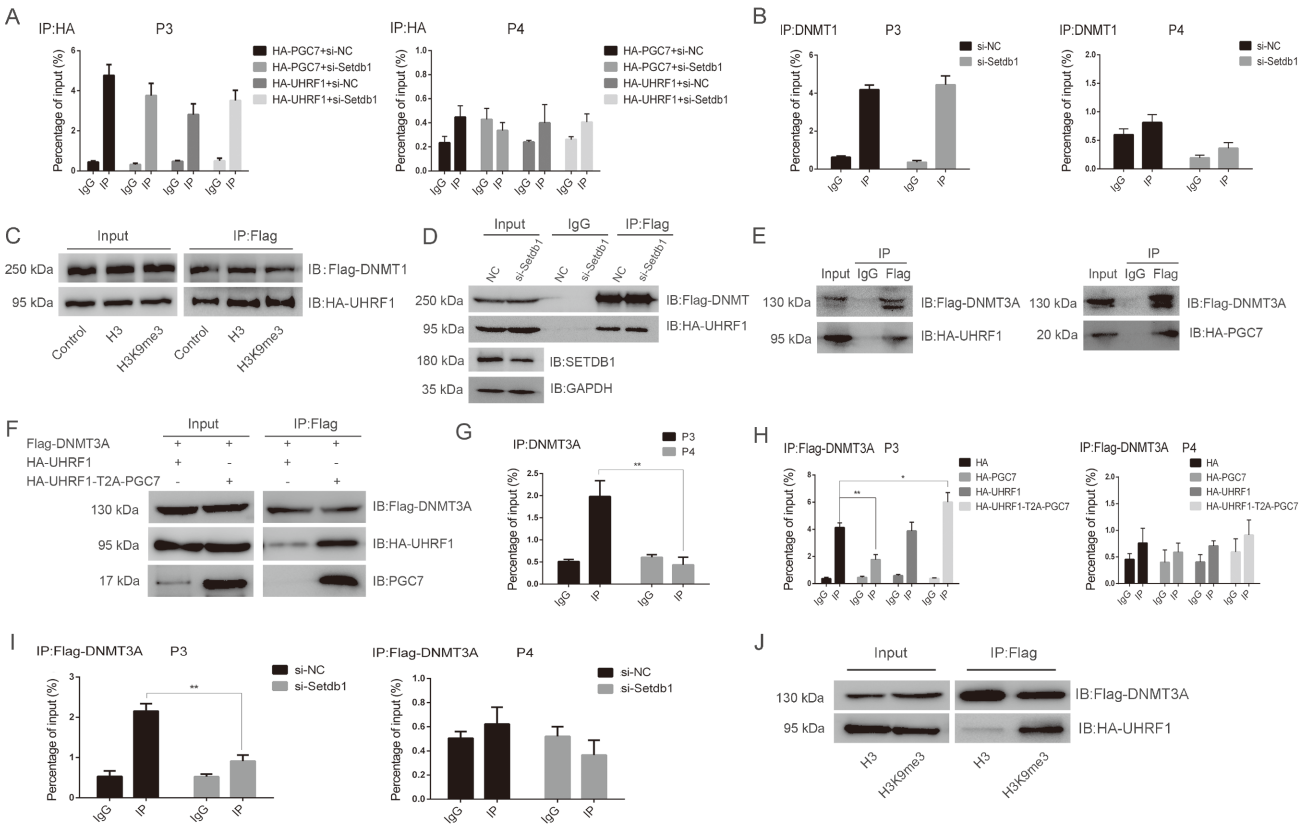

Figure 6. H3K9me3 enrichment is required for DNMT3A recruitment by UHRF1 (A,B) *Setdb1* knockdown did not affect the ability of PGC7, UHRF1 and DNMT1 to bind with the IG-DMR. F9 ECs were transfected with NC-siRNA or Setdb1-siRNA with pCMV-HA-UHRF1 or pCMV-HA-PGC7 as indicated. ChIP assay was performed using an anti-HA tag or DNMT1 antibody. Primers P3 and P4 were used to detect the binding ability of HA-tagged PGC7, HA-tagged UHRF1 or DNMT1 to the IG-DMR. Normal mouse IgG served as the negative control. (C)The interaction between DNMT1 and UHRF1 was improved by both L-H3 and L-H3K9me3. F9 ECs were transfected with pCMV-HA-UHRF1 and pCMV-Flag-DNMT1. After 48 h, N-biotinylated peptides containing 22 amino acids of the histone H3 N-terminal tail, named H3, H3K9me2, and H3K9me3, were added into the lysates. An anti-Flag tag antibody was used to capture protein-DNMT1 complexes. (D) *Setdb1* knockdown did not affect the interaction between DNMT1 and UHRF1. F9 ECs were transfected as indicated. An anti-Flag tag antibody was used to capture N-Flag-tagged protein-DNMT1 complexes. Normal mouse IgG served as the negative control. (E) DNMT3A interacted with PGC7 and UHRF1 in F9 ECs. (F) The presence of PGC7 enhanced the association of DNMT3A with UHRF1.The pCMV-Flag-DNMT3A and pCMV-HA-UHRF1 or pCMV-HA-UHRF1-T2A-PGC7 were transfected into F9 ECs as indicated. An anti-Flag tag antibody was used to capture N-Flag-tagged protein-DNMT3A complexes. (G) DNMT3A was specifically enriched at the IG-DMR P3 site. ChIP-qPCR analysis of Flag-tagged DNMT3A in F9 ECs. Normal mouse IgG served as the negative control. (H) The enrichment of DNMT3A was related to the interaction between PGC7 and UHRF1. F9 ECs were transfected as indicated. ChIP assay was performed using an anti-Flag tag antibody. Primers P3 and P4 were used to detect the binding activity of DNMT3A to the IG-DMR. Normal mouse IgG served as the negative control. (I) *Setdb1* knockdown impaired the ability of DNMT3A to bind to the IG-DMR. F9 ECs were transfected with pCMV-Flag-DNMT3A and Setdb1-siRNA as indicated. ChIP assays were performed using an anti-Flag tag antibody. Primers P3 and P4 were used to detect the binding ability of DNMT3A to the IG-DMR. Normal mouse IgG served as the negative control. (J) The interaction between DNMT3A and UHRF1 was significantly improved by L-H3K9me3. F9 ECs were transfected with pCMV-HA-UHRF1 and pCMV-Flag-DNMT3A. After 48 h, N-biotinylated peptides containing 22 amino acids of the histone H3 N-terminal tail, named H3, H3K9me2, and H3K9me3 were added into the lysates. An anti-Flag tag antibody was used to capture protein-DNMT3A complexes.

recruitment of DNMT3A to the IG-DMR. ChIP-qPCR results supported this assumption, as DNMT3A was specifically enriched at the IG-DMR P3 site (Figure 6G), where PGC7 and UHRF1 were co-localized. ChIP-qPCR results showed that overexpression of both PGC7 and UHRF1 significantly increased DNMT3A enrichment at the P3 site in the IG-DMR (Figure 6H), indicating that the enrichment of DNMT3A is related to the interaction between PGC7 and UHRF1. Interestingly, PGC7 alone inhibited the binding of DNMT3A to the IG-DMR, which is consistent with the results from Xu *et al.* [17]. However, upon interaction with UHRF1, PGC7 promoted the recruitment of DNMT3A.

According to the results from Meilinger *et al.* [42], the recruitment of DNMT3A by UHRF1 requires prior H3K9 methylation. To investigate the effect of H3K9me3 on the recruitment of DNMT3A, ChIP-qPCR assays were performed after *Setdb1* knockdown. The reduction in H3K9me3 caused by *Setdb1* knockdown led to the expected reduction in DNMT3A enrichment at the P3 site (Figure 6I). In addition, we added L-H3 and L-H3K9me3 to cell lysates containing overexpressed UHRF1 and DNMT3A, and found that the interaction between DNMT3A and UHRF1 was significantly improved by L-H3K9me3, but not by L-H3 (Figure 6J), suggesting that H3K9me3 deposition enhances the ability of UHRF1 to recruit DNMT3A.

All these results demonstrated that the cooperative association of PGC7 and UHRF1 in the IG-DMR helps to recruit DNMT1 and to maintain DNA methylation in the IG-DMR. Moreover, the interaction between PGC7 and UHRF1 promotes the recruitment of the H3K9 methyltransferase SETDB1, which leads to H3K9me3 enrichment and further promotes the recruitment of DNMT3A by UHRF1, resulting in DNA hypermethylation in the IG-DMR and ultimately in the inhibition of the *Gtl2* gene expression (Supplementary Figure S4).

Discussion

The *Dlk1-Dio3* imprinted region is evolutionarily conserved in mammals. Balanced gene expression in the *Dlk1-Dio3* locus plays a pivotal role in cell growth and development. Loss of imprinting in this locus leads to Kagami-Ogata syndrome or Temple syndrome in humans, and to developmental defects and premature death in mice. In addition, the dysregulation of the *Dlk1-Dio3* locus is highly linked to various disorders such as cancers and to defects in somatic cell nuclear transfer. It is known that the IG-DMR is the major imprinting control region in the *Dlk1-Dio3* locus and aberrant DNA methylation in the IG-DMR is the main cause of imprinting dysregulation. However, the precise mechanisms underlying the regulation of imprinting in *Dlk1-Dio3* locus remain largely unknown.

In the present study, we used F9 EC cell line, in which the IG-DMR is hypermethylated, as a cell model to investigate the mechanisms by which the interaction between PGC7 and UHRF1 contributes to the imprinting regulation. The F9 EC cell line is derived from a mouse testicular teratoma that originated from pluripotent germ cells. It is used as a model for cell differentiation research because of its ability to differentiate into endodermal-like derivatives after treatment with retinoic acid. Moreover, because of its limited differentiation ability, F9 EC cells can also be considered as representative of low pluripotent stem cells. Given that F9 EC cell line is derived from testicular teratomas, it is a useful tool for investigating pluripotency, differentiation, and tumorigenesis. Understanding the mechanisms of imprinting dysregulation in F9 EC cells will not only improve our understanding of imprinting regulation but might also allow to identify means to prevent imprinting aberrance in iPSC production, tumorigenesis, and somatic cell nuclear transfer.

PGC7 is specifically expressed in primordial germ cells, oocytes, pluripotent stem cells, and testicular germ tumor cells. It mainly functions by modulating chromatin condensation and epigenetic modifications in early embryonic cells. Previously, we predicted that PGC7 is an entirely IDP based on its amino acid sequence. IDPs, including PGC7, have fully disordered structures and fail to form a stable conformation, yet they exhibit biological activities through interaction with other molecules and exist *in vivo* in various protein complexes defined by different interacting partners or different cell contexts. Therefore, we speculated that the diverse functions of PGC7 depend on its various interaction partners or different cell contexts. We identified 291 potential PGC7-interacting proteins, supporting the knowledge that one IDP displays conformation changes and binds to many different partners. According to the particular functions of the interacting partners, we linked PGC7 to critical cellular processes including translation, RNA processing, cell cycle, and regulation of heterochromatin structure.

UHRF1, one of the 291 PGC7 interaction candidates, is an indispensible intermediate for DNMT1-mediated maintenance of DNA methylation at the hemimethylated CpG dinucleotides sites generated during the DNA replication process. Because their functions are relevant to the maintenance of DNA methylation, we deduced that PGC7 and UHRF1 might work together in regulating local DNA methylation. PGC7 and UHRF1 co-localize at specific chromatin regions, indicating that PGC7 and UHRF1 function cooperatively only at specific genomic loci without affecting the global DNA methylation level and maintenance of cell pluripotency. The strategy for identifying these specific genomic sites is based on the assumption that the effect of PGC7 and UHRF1 on the expression of specific genes should be synergistic. The results from Xu *et al.* [17] showed that PGC7 binds to the IG-DMR in mESC. Although there is no evidence that UHRF1 binds to the IG-DMR, it was reported that UHRF1 protein level and the expression of the *Gtl2* gene are negatively correlated in hepatocellular carcinoma cells [22]. All these data suggested that PGC7 and UHRF1 work together in the IG-DMR of the *Dlk1-Dio3* imprinted region, which was confirmed by ChIP-qPCR assay.

The bisulfite sequencing assay indicated that the interaction of PGC7 with UHRF1 is involved in the regulation of DNA methylation in the IG-DMR. We made two noteworthy observations. First, the IG-DMR is hypermethylated to nearly 90% in F9 ECs, which might be responsible for the relative low-level expression of *Gtl2* lncRNA. Second, when PGC7 and UHRF1 were co-overexpressed in cells, the DNA methylation level of the IG-DMR was further increased to nearly 100%, which might induce the recruitment of *de novo* transmethylase DNMT3A.

The DNA methyltransferase DNMT1 is the major UHRF1-interacting partner involved in DNA methylation maintenance. The co-IP assay results indicated that PGC7 does not directly interact with DNMT1 but instead recruits DNMT1 through its interaction with UHRF1. Furthermore, upon knockdown of *UHRF1*, DNMT1 enrichment in the IG-DMR was completely disrupted. These results led to the conclusion that the recruitment of DNMT1 is directly mediated by UHRF1, while the role of PGC7 is mainly to promote the binding of UHRF1 to the IG-DMR.

It was reported that UHRF1 binds to H3K9me2/3, whereas PGC7 binds to H3K9me2 [16,37]. It is reasonable to speculate that H3K9me2 promotes the interaction between PGC7 and UHRF1. The results of pulldown assay *in vitro* indicated that the histone H3 N-terminal tail increases the interaction of PGC7 with UHRF1. Interestingly, when associated with UHRF1, PGC7 is more inclined to bind with H3K9me3. Since the binding properties of UHRF1 did not change, we speculated that PGC7 tends to interact with UHRF1 bound to H3K9me3, or that PGC7 prefers to bind with H3K9me3 because of the conformation change induced by UHRF1. The local co-localization of PGC7 and H3K9me3 results presented in Figures 2B and 4C also supported the hypothesis that the binding of PGC7 to H3K9me3 depends on UHRF1. Interestingly, H3K9me2 is enriched at the P4 site but not at the P3 site. This may be because the initial recruitment of PGC7 and UHRF1 requires H3K9me2 deposition at the P3 site, which is subsequently converted into H3K9me3 after SETDB1 recruitment.

UHRF1 recruits the H3K9 methyltransferases G9a and SETDB1. PGC7 blocks the interaction between UHRF1 and G9a. In contrast, PGC7 directly interacts with SETDB1 and enhances the interaction between UHRF1 and SETDB1. ChIP-qPCR assay confirmed that SETDB1 recruitment is linked to both PGC7 and UHRF1, and contributes to the enrichment of H3K9me3 in the IG-DMR. Interestingly, we found that in the absence of UHRF1, PGC7 directly interacted with SETDB1, which we identified as a potential PGC7-interacting protein [20]. Furthermore, the immunofluorescence data showed that UHRF1 and SETDB1 were partially co-localized in the nucleus, whereas PGC7 and SETDB1 almost completely co-localized (Supplementary Figure S5). These results further supported that PGC7 interacts with SETDB1 independently of UHRF1. This interaction has two possible consequences. Indeed, SETDB1 might be recruited by PGC7 to convert PGC7-associated H3K9me2 to H3K9me3 or PGC7 might inhibit SETDB1 activity to maintain its association with H3K9me2.

The finding that the suppression of SETDB1 led to a decrease of DNA methylation in the IG-DMR suggested that the reduction of H3K9me3 level impairs the recruitment of DNA transmethylases. Our most interesting finding was that H3K9me3 promoted the recruitment of DNMT3A, but not DNMT1, by UHRF1, as shown by co-IP and ChIP-qPCR assays. In addition, it was worth noting that PGC7 interacted with DNMT3A and inhibited the enrichment of DNMT3A in the IG-DMR, which is consistent with previous reports. However, the interaction of PGC7 with UHRF1 enhanced the recruitment of DNMT3A. We speculated that UHRF1 induces PGC7 conformation changes to promote the recruitment of DNMT3A. In the absence of UHRF1, other interaction partners may disrupt the interaction between PGC7 and DNMT3A, and thus inhibiting DNMT3A recruitment.

Several research groups have reported the biological functions of the interaction between PGC7 and UHRF1. Our results obtained in F9 ECs conflict with those of others in several aspects. PGC7 had no effect on the intrinsic nuclear localization of UHRF1 in F9 ECs. Du *et al.* [43] reported that nuclear PGC7 disturbs the recruitment of UHRF1 by the histone H3 tail and dissociates UHRF1 from chromatin in HEK-293T cells. In contrast, our results showed that PGC7 and UHRF1 co-localize in the IG-DMR of the *Dlk1-Dio3* locus in F9 ECs. The interaction between PGC7 and UHRF1 enhances their respective binding ability to histone H3 and even triggers H3K9me3 enrichment within the IG-DMR in a SETDB1-dependent manner. It remains to be determined whether these contradictory data are resulted from different cell contexts or from unidentified interaction partners of the PGC7-UHRF1 complex based on PGC7 disordered structure.

Finally, our results suggested that DNA hypermethylation in the IG-DMR in F9 ECs is induced by the interaction between PGC7 and UHRF1, which leads to recruitment of both DNMT1 and DNMT3A to this region (Figure 7). Since the potential *de novo* function of DNMT1 *in vivo* has previously been reported [30, 44], it remains to be clarified whether the hypermethylation of the IG-DMR mediated by PGC7 and UHRF1 is established by the canonical *de novo*

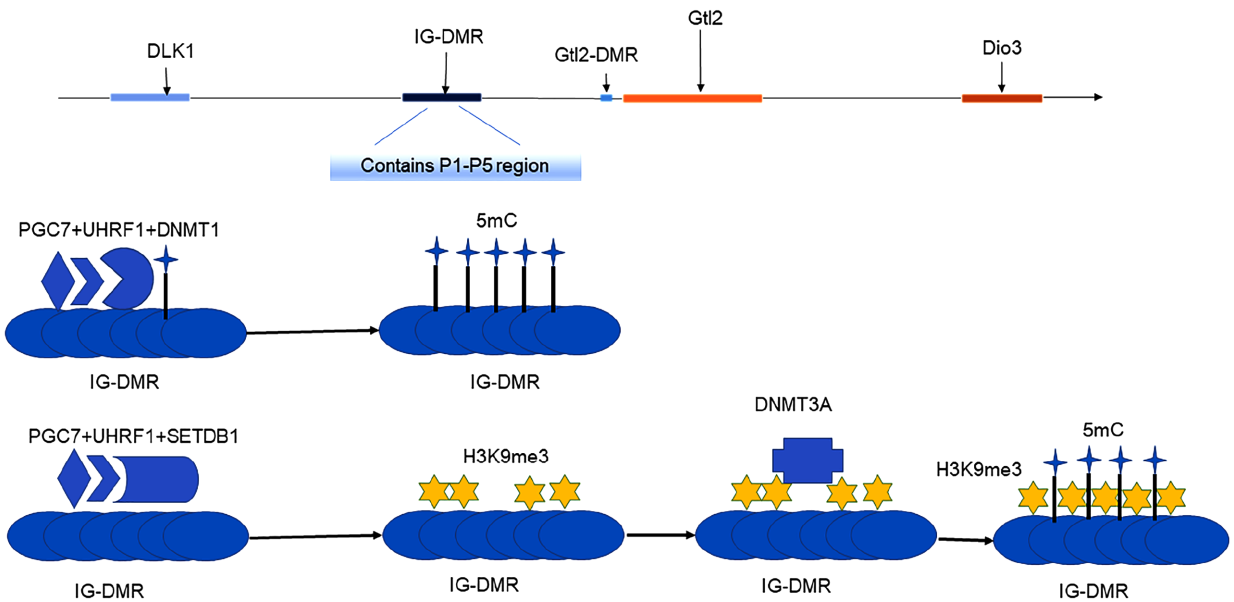

Figure 7. A schematic diagram of this study In F9 ECs, PGC7 and UHRF1 synergistically bind to IG-DMR within the *Dlk1-Dio3* imprinted locus. PGC7 strengthens UHRF1-mediated recruitment of both DNMT1 and SETDB1, resulting in maintenance of DNA methylation and further enrichment of H3K9me3 modification. Subsequently, DNMT3A recognizes H3K9me3 and facilitates DNA hypermethylation in IG-DMR.

transmethylase DNMT3A only, or whether DNMT1 is also involved in this process. Our results strongly support the latter because DNMT1 overexpression slightly increased DNA methylation in the IG-DMR. Our results also suggested that inhibiting the expression level of UHRF1 or promoting its nuclear export might be beneficial for preventing the imprinting dysregulation of the IG-DMR.

Supplementary Data

Supplementary data is available at *Acta Biochimica et Biophysica Sinica* online.

Funding

This work was supported by the grants from the National Natural Science Foundation of China (Nos. 31572405 and 31172279) and the Key Science and Technology Innovation Team in Shaanxi Province (No. 2014KCT-26) to Z.G.

Conflict of Interest

The authors declare that they have no conflict of interest.

References

1. Takada S, Tevendale M, Baker J, Georgiades P, Campbell E, Freeman T, Johnson MH, *et al.* Delta-like and gtl2 are reciprocally expressed, differentially methylated linked imprinted genes on mouse chromosome 12. *Curr Biol* 2000, 10: 1135–1138
2. Takada S, Paulsen M, Tevendale M, Tsai CE, Kelsey G, Cattanach BM, Ferguson-Smith AC. Epigenetic analysis of the Dlk1-Gtl2 imprinted domain on mouse chromosome 12: implications for imprinting control from comparison with Igf2-H19. *Hum Mol Genet* 2002, 11: 77–86
3. Siddiqi SA, Kumar NS, St. Hilaire RJ, Nutting DF, Mansbach Ii CM. Nutrient absorption. *Curr Opin Gastroenterol* 2000, 16: 147–153
4. He Y, Luo Y, Liang B, Ye L, Lu G, He W. Potential applications of MEG3 in cancer diagnosis and prognosis. *Oncotarget* 2017, 8: 73282–73295
5. Benetatos L, Vartholomatos G, Hatzimichael E. DLK1-DIO3 imprinted cluster in induced pluripotency: landscape in the mist. *Cell Mol Life Sci* 2014, 71: 4421–4430
6. Nady N, Lemak A, Walker JR, Avvakumov GV, Kareta MS, Achour M, Xue S, *et al.* Recognition of multivalent histone states associated with heterochromatin by UHRF1 protein. *J Biol Chem* 2011, 286: 24300–24311
7. Liu L, Luo GZ, Yang W, Zhao X, Zheng Q, Lv Z, Li W, *et al.* Activation of the imprinted Dlk1-Dio3 region correlates with pluripotency levels of mouse stem cells. *J Biol Chem* 2010, 285: 19483–19490
8. Sheik Mohamed J, Gaughwin PM, Lim B, Robson P, Lipovich L. Conserved long noncoding RNAs transcriptionally regulated by Oct4 and Nanog modulate pluripotency in mouse embryonic stem cells. *RNA* 2010, 16: 324–337
9. Guttman M, Donaghey J, Carey BW, Garber M, Grenier JK, Munson G, Young G, *et al.* lincRNAs act in the circuitry controlling pluripotency and differentiation. *Nature* 2011, 477: 295–300
10. Peng F, Li TT, Wang KL, Xiao GQ, Wang JH, Zhao HD, Kang ZJ, *et al.* H19/let-7/LIN28 reciprocal negative regulatory circuit promotes breast cancer stem cell maintenance. *Cell Death Dis* 2018, 8: e2569
11. Hori N, Yamane M, Kouno K, Sato K. Induction of DNA demethylation depending on two sets of Sox2 and adjacent Oct3/4 binding sites (Sox-Oct motifs) within the mouse H19/insulin-like growth factor 2 (Igf2) imprinted control region. *J Biol Chem* 2012, 287: 44006–44016
12. Hori N, Nakano H, Takeuchi T, Kato H, Hamaguchi S, Oshimura M, Sato K. A dyad oct-binding sequence functions as a maintenance sequence for the unmethylated state within the H19/Igf2-imprinted control region. *J Biol Chem* 2002, 277: 27960–27967
13. Stadtfeld M, Apostolou E, Akutsu H, Fukuda A, Follett P, Natesan S, Kono T, *et al.* Aberrant silencing of imprinted genes on chromosome 12qF1 in mouse induced pluripotent stem cells. *Nature* 2010, 465: 175–181
14. Carey BW, Markoulaki S, Hanna JH, Faddah DA, Buganim Y, Kim J, Ganz K, *et al.* Reprogramming factor stoichiometry influences the epigenetic state and biological properties of induced pluripotent stem cells. *Cell Stem Cell* 2011, 9: 588–598
15. Zhao S, Xu J, Liu S, Cui K, Li Z, Liu N. Dppa3 in pluripotency maintenance of ES cells and early embryogenesis. *J Cell Biochem* 2019, 120: 4794–4799
16. Szabó PE, Pfeifer GP. H3K9me2 attracts PGC7 in the zygote to prevent Tet3-mediated oxidation of 5-methylcytosine. *J Mol Cell Biol* 2012, 4: 427–429
17. Xu X, Smorag L, Nakamura T, Kimura T, Dressel R, Fitzner A, Tan X, *et al.* Dppa3 expression is critical for generation of fully reprogrammed iPS cells and maintenance of Dlk1-Dio3 imprinting. *Nat Commun* 2015, 6: 6008
18. Ying QL, Wray J, Nichols J, Batlle-Morera L, Doble B, Woodgett J, Cohen P, *et al.* The ground state of embryonic stem cell self-renewal. *Nature* 2008, 453: 519–523
19. Ghimire S, Van der Jeught M, Neupane J, Roost MS, Anckaert J, Popovic M, Van Nieuwerburgh F, *et al.* Comparative analysis of naive, primed and ground state pluripotency in mouse embryonic stem cells originating from the same genetic background. *Sci Rep* 2018, 8: 5884
20. Liu H, Zhang L, Wei Q, Shi Z, Shi X, Du J, Huang C, *et al.* Comprehensive proteomic analysis of PGC7-interacting proteins. *J Proteome Res* 2017, 16: 3113–3123
21. Quenneville S, Verde G, Corsinotti A, Kapopoulou A, Jakobsson J, Offner S, Baglivo I, *et al.* In embryonic stem cells, ZFP57/KAP1 recognize a methylated hexanucleotide to affect chromatin and DNA methylation of imprinting control regions. *Mol Cell* 2011, 44: 361–372
22. Zhuo H, Tang J, Lin Z, Jiang R, Zhang X, Ji J, Wang P, *et al.* The aberrant expression of MEG3 regulated by UHRF1 predicts the prognosis of hepatocellular carcinoma. *Mol Carcinog* 2016, 55: 209–219
23. Unoki M, Nishidate T, Nakamura Y. ICBP90, an E2F-1 target, recruits HDAC1 and binds to methyl-CpG through its SRA domain. *Oncogene* 2004, 23: 7601–7610
24. Rottach A, Frauer C, Pichler G, Bonapace IM, Spada F, Leonhardt H. The multi-domain protein Np95 connects DNA methylation and histone modification. *Nucleic Acids Res* 2010, 38: 1796–1804
25. Rothbart SB, Dickson BM, Ong MS, Krajewski K, Houliston S, Kireev DB, Arrowsmith CH, *et al.* Multivalent histone engagement by the linked tandem Tudor and PHD domains of UHRF1 is required for the epigenetic inheritance of DNA methylation. *Genes Dev* 2013, 27: 1288–1298
26. Qin W, Wolf P, Liu N, Link S, Smets M, La Mastra F, Forné I, *et al.* DNA methylation requires a DNMT1 ubiquitin interacting motif (UIM) and histone ubiquitination. *Cell Res* 2015, 25: 911–929
27. Qian C, Li S, Jakoncic J, Zeng L, Walsh MJ, Zhou MM. Structure and hemimethylated CpG binding of the SRA domain from human UHRF1. *J Biol Chem* 2008, 283: 34490–34494
28. Ashraf W, Ibrahim A, Alhosin M, Zaayter L, Ouararhni K, Papin C, Ahmad T, *et al.* The epigenetic integrator UHRF1: on the road to become a universal biomarker for cancer. *Oncotarget* 2017, 8: 51946–51962
29. Funaki S, Nakamura T, Nakatani T, Umehara H, Nakashima H, Nakano T. Inhibition of maintenance DNA methylation by Stella. *Biochem Biophys Res Commun* 2014, 453: 455–460
30. Li Y, Zhang Z, Chen J, Liu W, Lai W, Liu B, Li X, *et al.* Stella safeguards the oocyte methylome by preventing *de novo* methylation mediated by DNMT1. *Nature* 2018, 564: 136–140

31. von Meyenn F, Iurlaro M, Habibi E, Liu NQ, Salehzadeh-Yazdi A, Santos F, Petrini E, *et al.* Impairment of DNA methylation maintenance is the main cause of global demethylation in naive embryonic stem cells. *Mol Cell* 2016, 62: 848–861
32. Graf U, Casanova EA, Wyck S, Dalcher D, Gatti M, Vollenweider E, Okoniewski MJ, *et al.* Pramel7 mediates ground-state pluripotency through proteasomal–epigenetic combined pathways. *Nat Cell Biol* 2017, 19: 763–773
33. Li QR, Xing XB, Chen TT, Li RX, Dai J, Sheng QH, Xin SM, *et al.* Large scale phosphoproteome profiles comprehensive features of mouse embryonic stem cells. *Mol Cell Proteomics* 2011, 10: M110.001750
34. Hirai H, Katoku-Kikyo N, Karian P, Firpo M, Kikyo N. Efficient iPS cell production with the MyoD transactivation domain in serum-free culture. *PLoS ONE* 2012, 7: e34149
35. Li Z, Fei T, Zhang J, Zhu G, Wang L, Lu D, Chi X, *et al.* BMP4 signaling acts via dual-specificity phosphatase 9 to control ERK activity in mouse embryonic stem cells. *Cell Stem Cell* 2012, 10: 171–182
36. Sanli I, Feil R. Chromatin mechanisms in the developmental control of imprinted gene expression. *Int J Biochem Cell Biol* 2015, 67: 139–147
37. Cheng J, Yang Y, Fang J, Xiao J, Zhu T, Chen F, Wang P, *et al.* Structural insight into coordinated recognition of trimethylated histone H3 lysine 9 (H3K9me3) by the plant homeodomain (PHD) and tandem tudor domain (TTD) of UHRF1 (ubiquitin-like, containing PHD and RING finger domains, 1) protein. *J Biol Chem* 2013, 288: 1329–1339
38. Kim JK, Estève PO, Jacobsen SE, Pradhan S. UHRF1 binds G9a and participates in p21 transcriptional regulation in mammalian cells. *Nucleic Acids Res* 2009, 37: 493–505
39. Sharif J, Endo TA, Nakayama M, Karimi MM, Shimada M, Katsuyama K, Goyal P, *et al.* Activation of endogenous retroviruses in Dnmt1−/− ESCs involves disruption of SETDB1-mediated repression by NP95 binding to hemimethylated DNA. *Cell Stem Cell* 2016, 19: 81–94
40. Wada S, Ideno H, Shimada A, Kamiunten T, Nakamura Y, Nakashima K, Kimura H, *et al.* H3K9MTase G9a is essential for the differentiation and growth of tenocytes *in vitro*. *Histochem Cell Biol* 2015, 144: 13–20
41. Patel DJ. A structural perspective on readout of epigenetic histone and DNA methylation marks. *Cold Spring Harb Perspect Biol* 2016, 8: a018754
42. Meilinger D, Fellinger K, Bultmann S, Rothbauer U, Bonapace IM, Klinkert WEF, Spada F, *et al.* Np95 interacts with *de novo* DNA methyltransferases, Dnmt3a and Dnmt3b, and mediates epigenetic silencing of the viral CMV promoter in embryonic stem cells. *EMBO Rep* 2009, 10: 1259–1264
43. Du W, Dong Q, Zhang Z, Liu B, Zhou T, Xu RM, Wang H, *et al.* Stella protein facilitates DNA demethylation by disrupting the chromatin association of the RING finger-type E3 ubiquitin ligase UHRF1. *J Biol Chem* 2019, 294: 8907–8917
44. Shirane K, Toh H, Kobayashi H, Miura F, Chiba H, Ito T, Kono T, *et al.* Mouse oocyte methylomes at base resolution reveal genome-wide accumulation of non-CpG methylation and role of DNA methyltransferases. *PLoS Genet* 2013, 9: e1003439